ChemComm

COMMUNICATION

View Article Online
View Journal | View Issue



Cite this: *Chem. Commun.*, 2025, **61**, 18432

Received 18th August 2025,
Accepted 16th October 2025

DOI: 10.1039/d5cc04769b

rsc.li/chemcomm

# Design strategies for single-molecule toroics in lanthanofullerene systems

Tanu Sharma and Gopalan Rajaraman *

**Single-molecule toroids (SMTs) present unique advantages over other classes of molecular magnets for proposed applications. However, stabilising toroidal moments in molecular systems remains a significant challenge. In this study, we demonstrate that by encapsulating a {$Dy_3$} motif within a series of fullerene cages ranging from $C_{94}$ to $C_{100}$, it is possible to achieve stable SMT behaviour. This work establishes fullerene-encapsulated SMTs as promising, device-ready molecular candidates for future technological applications.**

Single-molecule toroids (SMTs) represent a unique class of lanthanide-based molecular systems where the local magnetic axes adopt a vortex-like arrangement,[1] giving rise to toroidal magnetic moments rather than conventional dipoles.[2] This topology renders SMTs magnetically "silent" in homogeneous fields yet highly responsive to electric fields,[3] making them appealing candidates for quantum information storage, molecular spintronics, and magnetoelectric devices.[3,4] Unlike standard single-molecule magnets (SMMs), the toroidal arrangement suppresses quantum tunnelling of magnetisation, thereby offering enhanced stability and longer coherence times.

The first experiment in this area was in 2006, when $Dy_3$ triangular complexes were first shown to display anomalous S-shaped hysteresis and a near-vanishing ground-state moment.[5] Subsequent single-crystal magnetometry studies[6] provided direct evidence of chiral, tangential orientation of Dy anisotropy axes in such triangles, and high-level *ab initio* calculations demonstrated that the ground Kramers doublet corresponds to a toroidal arrangement of local magnetisations.[7] These studies marked the formal introduction of SMTs and demonstrated that toroidal moments can indeed be stabilised in lanthanide clusters. Since then, related motifs have been realised in rhombic and cubic $Dy_4$ clusters,[8–10] wheel-like $Dy_6$ assemblies,[11] and even 3d–4f heterometallic systems, highlighting the growing structural diversity. Nevertheless, SMTs remain rare because achieving precise control over the anisotropy axes of Dy(III) ions is highly nontrivial, and small distortions often suppress toroidal behaviour.[12] Retaining toroidal states upon surface immobilisation remains an even greater challenge due to the extreme sensitivity of Dy(III) anisotropy to its coordination environment.

A promising route to overcome these limitations is encapsulation of $Dy_3$ units inside fullerene cages, which can provide structural confinement, environmental protection, and reduced spin–phonon coupling while preserving the toroidal topology.[13–17] Experimentally, several trinuclear systems with different ligand-bridged clusterfullerenes have already been isolated, providing a clear precedent for our ligand choices. Notable examples include $Dy_3C_2$@Ih-$C_{80}$,[18] $Dy_3N$@$C_{80}$,[19] or it analogues[13] and $Dy_3$@$C_{98}$,[20] oxide-type systems such as $Sc_4(\mu_3\text{–}O)_2$@$C_{80}$[21] and $Ho_2O$@$C_{92}$,[22] cyanide-containing species like TbCN@$C_{82}$,[23] and more recently, fluoride-bridged clusters exemplified by $Gd_2F$@$C_{80}(CF_3)$.[24] These studies establish that O, CN, and F ligands can act as effective internal bridges to stabilise multimetallic clusters inside fullerene cages. In this work, we build on these experimental foundations and propose, through computational design, that embedding {$Dy_3$} units into larger fullerene cages ($C_{94}$–$C_{100}$) can orient the magnetic axes appropriately to stabilise genuine SMT states. Our study, therefore, provides a conceptual framework and design strategy to motivate synthetic efforts toward fullerene-stabilised SMTs.

Inspired by this concept, we computationally designed a series of $Dy_3$-based SMT models, starting from simpler open structures reported in the literature[25] and then exploring their encapsulation within fullerene cages. The $Dy_3X_3$ geometries were chosen to stabilise toroidal moments, requiring the Dy magnetic axes to lie roughly normal to the triangle radii. To this end, we systematically examined different bridging ligands ($O^{2-}$, $F^-$, $CN^-$) to identify the arrangements that best promote collinear and cyclic alignment of the anisotropic axes of the Dy(III) ion. The open complexes include: {$Dy_3(CN)_3(Cp)_6$} (**1**), {$Dy_3(H)_3(Cp)_6$} (**2**), {$Dy_3F_3(Cp)_3$}$^{+3}$ (**3**), {$Dy_3O_3(Cp)_3$} (**4**), and {$Dy_3O_3$(Cp-$SiMe_3$)$_3$} (**5**). Building on these, we investigated the encapsulation of selected {$Dy_3X_3$} cores within fullerene cages of varying sizes: {$Dy_3F_3$@$C_{100}$}$^{+1}$ (**6**), {$Dy_3O_3$@$C_{100}$}$^{+1}$ (**7**), {$Dy_3O_3$@$C_{98}$}$^{+1}$ (**8**), {$Dy_3O_3$@$C_{96}$}$^{+1}$ (**9**), and {$Dy_3F_3$@$C_{94}$}$^{+1}$ (**10**)

*Department of Chemistry, Indian Institute of Technology Bombay, Powai, Mumbai-400076, India. E-mail: rajaraman@chem.iitb.ac.in; Tel: +91-22-2576-7183*

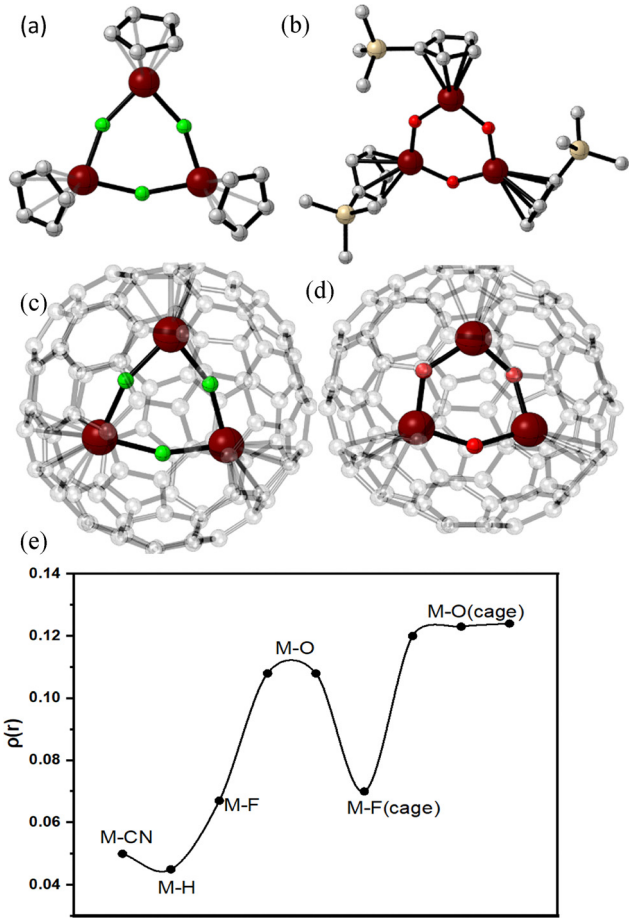


Fig. 1 DFT optimized structures of (a) **3** $\{Dy_3F_3(Cp)_3\}$, (b) **5** $\{Dy_3O_3(Cp\text{-}SiMe_3)_3\}$, (c) **6** $\{Dy_3F_3@C_{100}\}$ (d) **8** $\{Dy_3O_3@C_{98}\}$ and (e) plot showing $|\rho(r)|$ corresponding to metal–ligand bonds for various complexes. Color code: maroon – Dy, red – O, green– F, light grey – C, and ivory – Si, hydrogens are omitted for clarity.

(Fig. 1 and Fig. S1). Our goal was to examine how cage confinement affects the stability, geometry, and magnetic properties of SMTs, and to identify the minimum cage size required to retain the triangular $Dy_3$ configuration essential to exhibiting toroidal behaviour.

To gain insights into the nature of bonding within the $\{Dy_3X_3\}$ cores and between the metal centres and their surrounding environment (including cage and ligands), we performed Atoms in Molecules (AIM) analysis.

This topological analysis of electron density identified bond critical points (BCPs) in all $\{Dy_3X_3\}$ units, which represent localised regions of electron density corresponding to bonding interactions. The consistent presence and nature of these BCPs across different complexes confirm the existence of well-defined, albeit weak, bonding interactions within the $\{Dy_3X_3\}$ framework (see Table S1).

Despite the modest bond strengths, these interactions play a vital role in maintaining the structural coherence and electronic communication necessary for the overall stability and magnetic behaviour of these lanthanide systems.

In this study, we observed that the $|V(r)/G(r)|$ ratio (Table S1), Dy…cage interactions are predominantly ionic in nature as the ratio is found to be close to the value of 1. This is further supported by the positive values of $H(r)$, reinforcing the electrostatic nature of these interactions. When the $\rho(r)$ for various complexes are plotted, it shows that the highest $\rho(r)$ values are found in Dy–O bonds confined within cages, this is followed by Dy–O bonds outside of cages. The next highest $\rho(r)$ values are observed in Dy–F bonds, while Dy–H bonds exhibit the lowest $\rho(r)$ values. This indicates that the strength of metal–ligand bonds varies in the following order: Dy–O (cage) > Dy–O (non-cage) > Dy–F (cage) > Dy–F (non-cage) > Dy–CN > Dy–H. This hierarchy suggests that cage confinement significantly enhances the strength of Dy–O bonds, followed by non-caged Dy–O and Dy–F bonds, with Dy–CN and Dy–H bonds being the weakest among the ones studied.

To investigate the magnetic interactions within these systems, density functional theory (DFT) calculations were performed on all model complexes (refer to computational details in the SI). The exchange interactions were evaluated using the Hamiltonian described in eqn (S1), while dipolar couplings were computed using eqn (S2). All calculated exchange interactions were found to be antiferromagnetic and very weak in magnitude, which is typical for lanthanide-based systems. The angle between three Dy(III) ions $g_{zz}$ axis is $\sim 53^\circ$, suggesting that dipolar coupling is ferromagnetic in nature,[26] and this results in total magnetic coupling ($J_{tot}$) to be very weak and net ferromagnetic (Table 1 and Table S2). This is attributed to the highly shielded and localised nature of 4f orbitals, which minimises orbital overlap and consequently leads to small

Table 1 Computed deviation from the out-of-plane angle ($\theta$), deviation from the tangent (canting angle ($\phi$)) and first excited-state energy gap across all complexes for Dy1, Dy2, and Dy3 centres

| Molecule | $\theta_1$ (°) | $\theta_2$ (°) | $\theta_3$ (°) | $\varphi_1$ (°) | $\varphi_2$ (°) | $\varphi_3$(°) | $J_{exc}$ ($cm^{-1}$) | $J_{dip}$ ($cm^{-1}$) | $J_{tot}$ ($cm^{-1}$) | $\Delta E$ ($cm^{-1}$) |
|---|---|---|---|---|---|---|---|---|---|---|
| **1** | 89.2 | 89.7 | 89.4 | 89.3 | 90.2 | 90.6 | −0.022 | 0.119 | 0.097 | 342.1 |
| **2** | 89.9 | 89.9 | 89.9 | 90.0 | 89.9 | 90.1 | −0.488 | 0.343 | −0.145 | 212.3 |
| **3** | 24.7 | 24.6 | 24.3 | 41.7 | 43.4 | 43.5 | −0.026 | 0.317 | 0.291 | 155.2 |
| **4** | 0.1 | 0.0 | 0.1 | 0.1 | 0.0 | 0.1 | −0.181 | 0.307 | 0.126 | 67.3 |
| **5** | 0.3 | 1.1 | 0.2 | 0.3 | 4.2 | 0.3 | −0.177 | 0.309 | 0.132 | 65.4 |
| **6** | 8.8 | 16.3 | 12.3 | 12.2 | 29.3 | 18.6 | −0.026 | 0.308 | 0.282 | 146.8 |
| **7** | 29.0 | 0.3 | 30.8 | 31.4 | 0.3 | 31.9 | −0.180 | 0.408 | 0.228 | 86.6 |
| **8** | 1.2 | 0.1 | 1.3 | 2.2 | 0.3 | 1.6 | −0.201 | 0.471 | 0.270 | 156.7 |
| **9** | 17.4 | 3.1 | 7.9 | 17.9 | 3.2 | 11.1 | −0.216 | 0.374 | 0.158 | 80.4 |

superexchange pathways. In typical toroidal systems, relatively weak but non-negligible exchange couplings are desirable to preserve local anisotropy, while enabling the subtle inter-ion interactions necessary for collective toroidal states. In the current series of complexes studied, **4** and **5** exhibit relatively weak total exchange interaction strengths $J_{tot} \approx 0.126$ cm$^{-1}$ and 0.132 cm$^{-1}$, respectively. Complexes **7**, **8**, and **9** show slightly higher $J_{tot}$ values in the range of 0.15–0.27 cm$^{-1}$, still within the moderate regime, suggesting they may support a weakly coupled network (Table 1 and Table S2).

Further CASSCF/RASSI-SO/SINGLE_ANISO calculations were performed in order to establish the magnetic properties in these systems (see computational details in SI). As shown in Table S3, complexes **1** and **2** have higher energy gaps (KD1-KD2 energy gap, $\Delta E \approx$ 212–342 cm$^{-1}$) than the other complexes with minimal variation in their individual *J*-values, supporting well-isolated Ising-like ground states rather than toroidal configurations. This pronounced separation can be directly attributed to the presence of two cyclopentadienyl (Cp) rings coordinated symmetrically around the Dy(III) center, which creates a strong axial crystal field. In contrast, the other complexes, lacking such strong axial ligation, exhibit considerably smaller KD1–KD2 separations. Among complexes **3** to **6**, complex **3** displays the largest gap, closely followed by complex **6**. This similarity in energy splitting aligns well with their comparable coordination geometries and ligand field environments, reinforcing the influence of subtle structural features on the crystal field splitting. When turning to the caged trinuclear $Dy_3$ systems (complexes **7–9**), a general trend of lower KD1–KD2 gaps is observed. Although the KD1–KD2 gap is lower in these complexes, they have a high KD1–KD8 gap. This may be due to increased structural flexibility and reduced axiality within the multicentered framework, which typically leads to enhanced mixing of excited states and a narrower separation of the doublets. However, complex **8** is a notable exception within this series. It exhibits the highest KD1–KD8 gap not only among the $Dy_3$ complexes but across the entire dataset. This remarkable energy separation suggests that the structural and electronic configuration around the Dy(III) centers in complex **8** is exceptionally well-suited for maximising anisotropy and minimising $M_J$ state mixing.

The computed ground-state anisotropic g-tensors components ($g_{xx}$, $g_{yy}$, $g_{zz}$) for the Dy1, Dy2, and Dy3 centers (Table S4) further reveal the nature of magnetic anisotropy in these complexes. In all nine systems, the Dy centres retain strong axial anisotropy, with $g_{zz}$ values significantly larger than $g_{xx}$ and $g_{yy}$, indicating Ising-type behaviour. However, the magnitude of these anisotropies and the transverse components vary across the series. Complexes **1–3** are characterised by nearly ideal Ising anisotropy with $g_{zz} \approx 19.9$ and negligible $g_{xx}/g_{yy}$ values ($\leq$0.003), suggesting highly collinear magnetic axes across all Dy centres. On the other hand, complexes **4** and **5** display slightly reduced $g_{zz}$ values ($\approx$15.8–16.9) along with non-zero transverse components ($g_{xx}/g_{yy}$ up to 4.2), implying tilted local anisotropy axes. Similarly, in complexes **7**, **8**, and **9**, although the $g_{zz}$ values remain high ($\approx$14.7–19.7), the transverse components are sufficiently large, suggesting a lack of true Ising anisotropy.

In the next step, we have employed POLY_ANISO simulation[17,18] to understand the magnetic properties of the coupled {$Dy_3$} system. For toroidal systems as mentioned earlier,[3] the out-of-plane angle ($\theta$), deviation from the tangent (canting angle, ($\varphi$) are two key parameters that control the metrics of toroidal moments (Table 1 and Fig. 2). In complexes **1** and **2**, all three Dy centres exhibit $\theta$ values close to 90°, indicating that their anisotropy axes are perfectly perpendicular to the $Dy_3$ plane. Moreover, the $\varphi$ angles between the axes are also ~90°, suggesting a collinear or nearly parallel axial alignment of the moments (Fig. S2). This clearly suggests that these compounds are not expected to show net toroidal behaviour. In contrast, complex **3** displays moderate tilting, with $\theta$ values around 24°, and $\varphi$ values in the range of 41–44°, indicating a non-collinear arrangement with no clear axial or net toroidal behaviour.

Complexes **4** and **5** present near-ideal conditions for SMTs. The $\theta$ values are nearly zero, confirming that the anisotropy axes lie entirely in the $Dy_3$ pl ane, while the $\varphi$ angles are also very small (below 5°), indicating minimal canting between the axes. This results in a triangular, in-plane alignment of the $g_{zz}$ axes, a hallmark of net toroidal systems (Fig. S2). Similarly, complex **8** shows an almost identical angular pattern, with $\theta$ and $\varphi$ values close to zero, suggesting the possibility of observing SMT characteristics. Complex **7** shows an asymmetric case: Dy2 lies nearly in the plane ($\theta \approx 0.3°$), while Dy1 and Dy3 are tilted out by about 30°. The corresponding $\varphi$ values suggest a bent or V-shaped arrangement, likely still able to support mixed toroidal characteristics. Complex **9** demonstrates moderate $\theta$ (3–17°) and $\varphi$ (3–18°) angles, indicating favourable mixed SMT effects, while **6** exhibits intermediate characteristics with $\theta$ = 8–16° and $\varphi$ up to 29°, also a probable candidate for mixed SMT regime.

In complexes **1**, **2**, **3** and **6**, the orientations of the $g_{zz}$ vectors are not aligned in a cyclic manner. In contrast, in complexes **4–9**, with the exception of **6**, exhibit a distinct cyclic arrangement of their $g_{zz}$ axes, either clockwise or counterclockwise, around the $Dy_3$ triangle. This coherent circulation of anisotropy axes is a hallmark of toroidal magnetism and suggests that these complexes may support toroidal magnetic moments. Such arrangements lead to cancellation of net magnetic dipole moments while preserving higher-order toroidal components, making these systems potential candidates for magnetoelectric or non-dipolar magnetic behaviour.

The first excited state in complexes **4**, **5**, **7**, **8** and **9** lies at 2.2, 2.0, 1.8, 3.3 and 2.3 cm$^{-1}$, from the ground state, respectively (Fig. 3 and Fig. S2, S3). These values suggest that significant

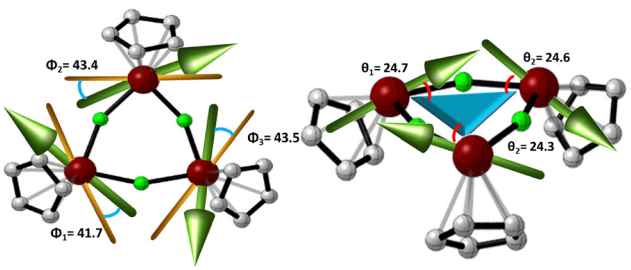


Fig. 2 Geometry of **3** exhibiting canting angle $\varphi$ (left) and out-of-plane angle $\theta$.

 

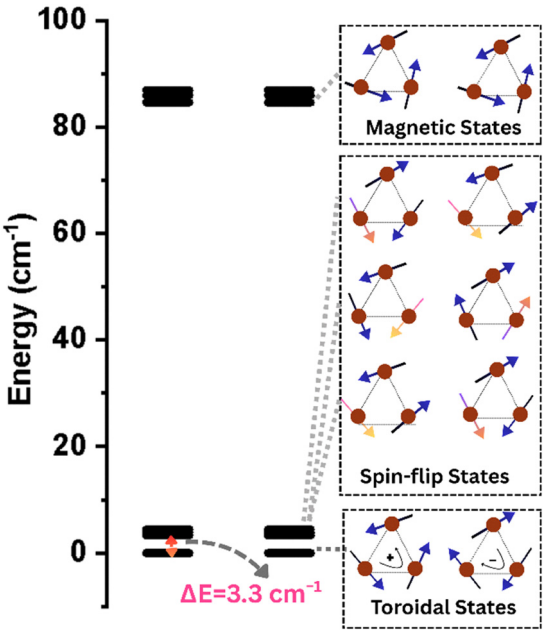


Fig. 3 Low-lying energy states, and Zeeman spectrum using the POLY_ANISO Lines for complex **8**.

interaction of the molecule with the cage, particularly in the $C_{98}$ cage.

The encapsulation of the $\{Dy_3O_3\}$ moiety inside the $C_{98}$ cage results in an increased gap of the ground-first-excited exchange-coupled state. Similarly, the total magnetic moment in the ground exchange pseudo-doublet state ($\mu_z$ = 1/2 $g_z\mu_B$) is calculated as 2.9, 3.2, 5.6, 10.7 and 6.6 $\mu_B$, for **4**, **5**, **7**, **8** and **9**, respectively (Fig. S3). These values align with the nonzero magnetisation observed at low temperatures, consistent with earlier studies on $\{Dy_3\}$ triangles and their characteristic magnetic behaviour.

Despite low yields and synthetic challenges, experimental precedents show that $\{Dy_3X_3\}$ clusters can form, be isolated, and characterised, supporting our computationally designed motifs as chemically realistic and experimentally plausible targets for stabilising toroidal moments. While there are several fullerene isomers exist, the SMT behaviour predicted are largely governed by the $\{Dy_3X_3\}$ cluster and strongly electronegative bridging ligands ($O^{2-}$/$F^-$), making the results relatively insensitive to minor variations in cage geometry.

To this end, we employed a combined DFT and *ab initio* CASSCF approach to systematically screen $\{Dy_3O_3\}$ triangular clusters encapsulated in diverse fullerene cages. Among the tested systems, $\{Dy_3O_3\}@C_n$ ($n$ = 96, 98, 100) emerged as promising single-molecule toroics (SMTs), with $C_{98}$ and $C_{100}$ showing optimal SMT characteristics. These findings underscore fullerene confinement as a robust strategy for stabilising SMTs, paving the way for their integration into quantum and spintronic devices.

## Conflicts of interest

There are no conflicts to declare.

## Data availability

The data supporting this article have been included as part of the supplementary information (SI). Supplementary information contains computational details, tables and figures corresponding to exchange coupling constants, magnetic anisotropy and relaxation mechanisms. See DOI: **https://doi.org/10.1039/d5cc04769b**.

## References

1 Q. Zhang, M. L. Baker, S. Li, M. P. Sarachik, J. J. Baldoví, A. Gaita-Ariño, E. Coronado, D. I. Alexandropoulos and T. C. Stamatatos, *Nanoscale*, 2019, **11**, 15131–15138.
2 K. R. Vignesh, S. K. Langley, A. Swain, B. Moubaraki, M. Damjanović, W. Wernsdorfer, G. Rajaraman and K. S. Murray, *Angew. Chem.*, 2018, **130**, 787–792.
3 L. Ungur, S.-Y. Lin, J. Tang and L. F. Chibotaru, *Chem. Soc. Rev.*, 2014, **43**, 6894–6905.
4 X. L. Li, Z. Ma and J. Tang, *Chem. – Eur. J.*, 2024, **30**, e202304369.
5 J. Tang, I. Hewitt, N. Madhu, G. Chastanet, W. Wernsdorfer, C. E. Anson, C. Benelli, R. Sessoli and A. K. Powell, *Angew. Chem., Int. Ed.*, 2006, **45**, 1729–1732.
6 J. Luzon, K. Bernot, I. J. Hewitt, C. E. Anson, A. K. Powell and R. Sessoli, *Phys. Rev. Lett.*, 2008, **100**, 247205.
7 L. F. Chibotaru, L. Ungur and A. Soncini, *Angew. Chem.*, 2008, **120**, 4194–4197.
8 P.-H. Guo, J.-L. Liu, Z.-M. Zhang, L. Ungur, L. F. Chibotaru, J.-D. Leng, F.-S. Guo and M.-L. Tong, *Inorg. Chem.*, 2012, **51**, 1233–1235.
9 C. Das, S. Vaidya, T. Gupta, J. M. Frost, M. Righi, E. K. Brechin, M. Affronte, G. Rajaraman and M. Shanmugam, *Chem. – Eur. J.*, 2015, **21**, 15639–15650.
10 A. Popov, D. Plokhov and A. Zvezdin, *Phys. Rev. B*, 2016, **94**, 184408.
11 L. Ungur, S. K. Langley, T. N. Hooper, B. Moubaraki, E. K. Brechin, K. S. Murray and L. F. Chibotaru, *J. Am. Chem. Soc.*, 2012, **134**, 18554–18557.
12 D. Chauhan, R. K. Tiwari and G. Rajaraman, *Small*, 2025, **21**, 2412283.
13 L. Spree, C. Schlesier, A. Kostanyan, R. Westerström, T. Greber, B. Büchner, S. M. Avdoshenko and A. A. Popov, *Chem. – Eur. J.*, 2020, **26**, 2436–2449.
14 G. Velkos, W. Yang, Y.-R. Yao, S. M. Sudarkova, F. Liu, S. M. Avdoshenko, N. Chen and A. A. Popov, *Chem. Commun.*, 2022, **58**, 7164–7167.
15 T. Sharma, R. K. Tiwari, S. Dey, A. Mariano, A. Lunghi and G. Rajaraman, *Chem. Sci.*, 2025, **16**, 13012–13021.
16 S. Mondal and A. Lunghi, *J. Am. Chem. Soc.*, 2022, **144**, 22965–22975.
17 S. Dey, T. Sharma and G. Rajaraman, *Chem. Sci.*, 2024, **15**, 6465–6477.
18 F. Jin, J. Xin, R. Guan, X.-M. Xie, M. Chen, Q. Zhang, A. A. Popov, S.-Y. Xie and S. Yang, *Chem. Sci.*, 2021, **12**, 6890–6895.
19 S. Yang, S. I. Troyanov, A. A. Popov, M. Krause and L. Dunsch, *J. Am. Chem. Soc.*, 2006, **128**, 16733–16739.
20 W. Fu, J. Zhang, H. Champion, T. Fuhrer, H. Azuremendi, T. Zuo, J. Zhang, K. Harich and H. C. Dorn, *Inorg. Chem.*, 2011, **50**, 4256–4259.
21 B. Q. Mercado, M. M. Olmstead, C. M. Beavers, M. L. Easterling, S. Stevenson, M. A. Mackey, C. E. Coumbe, J. D. Phillips, J. P. Phillips and J. M. Poblet, *Chem. Commun.*, 2010, **46**, 279–281.
22 Y. Yu, Z. Slanina, F. Wang, Y. Yang, Y. Lian, F. Uhlik, B. Xin and L. Feng, *Inorg. Chem.*, 2020, **59**, 11020–11027.
23 F. Liu, S. Wang, J. Guan, T. Wei, M. Zeng and S. Yang, *Inorg. Chem.*, 2014, **53**, 5201–5205.
24 Y. Zhao, Z. Hu, P. Chuai, H. Jin, S. Yang, J. Su and Z. Shi, *J. Am. Chem. Soc.*, 2024, **146**, 17003–17008.
25 Y. Obora, T. Ohta, C. L. Stern and T. J. Marks, *J. Am. Chem. Soc.*, 1997, **119**, 3745–3755.
26 J.-D. Leng, J.-L. Liu, W.-Q. Lin, S. Gómez-Coca, D. Aravena, E. Ruiz and M.-L. Tong, *Chem. Commun.*, 2013, **49**, 9341–9343.